# Capillary-Induced Contact Guidance

Steven Lenhert,*[,†,‡,¶] Ane Sesma,[§] Michael Hirtz,[‡] Lifeng Chi,[‡] Harald Fuchs,[‡] Hans Peter Wiesmann,[†] Anne E. Osbourn,[§] and Bruno M. Moerschbacher[¶]

*Klinik und Poliklinik für Mund- und Kiefer-Gesichtschirurgie, Universitätsklinikum Münster, Waldeyerstrasse 30, 48149 Münster, Germany, Physikalisches Institut, Westfälische Wilhelms-Universität, Wilhelm Klemm Strasse 10, and Center for Nanotechnology (CeNTech), 48149 Münster, Germany, Institut für Biochemie und Biotechnologie der Pflanzen, Westfälische Wilhelms-Universität, Hindenburgplatz 55, 48143 Münster, Germany, and John Innes Centre, Colney Lane, Norwich NR4 7UH, United Kingdom*

*Received April 11, 2007. In Final Form: July 9, 2007*

Topographical features are known to impose capillary forces on liquid droplets, and this phenomenon is exploited in applications such as printing, coatings, textiles and microfluidics. Surface topographies also influence the behavior of biological cells (i.e., contact guidance), with implications ranging from medicine to agriculture. An accurate physical description of how cells detect and respond to surface topographies is necessary in order to move beyond a purely heuristic approach to optimizing the topographies of biomaterial interfaces. Here, we have used a combination of Langmuir−Blodgett lithography and nanoimprinting to generate a range of synthetic microstructured surfaces with grooves of subcellular dimensions in order to investigate the influence of capillary forces on the biological process of contact guidance. The physical−chemical properties of these surfaces were assessed by measuring the anisotropic spreading of sessile water droplets. Having established the physical properties of each surface, we then investigated the influence of capillary forces on the processes of cellular contact guidance in biological organisms, using mammalian osteoblasts and germinating fungal spores as tester organisms. Our results demonstrate that capillary effects are present in topographical contact guidance and should therefore be considered in any physical model that seeks to predict how cells will respond to a particular surface topography.

## Introduction

Cell adhesion is a fundamental biological process that provides a challenge for physical adhesion theory because of the complex molecular machinery that is characteristic of living systems. Unlike the ideal wetting of a pure liquid drop on a smooth surface, cell adhesion involves factors such as membrane elasticity, cytoskeletal tension, and the dynamic properties of adhesive molecules on the cell surface.[1−6] These differences make it impractical to determine an interfacial energy for a living cell based on contact angles, as is often done in the wetting of pure liquid droplets. However, in the context of capillary theory, it is possible to determine certain linear relations between topography and the shape of liquid interfaces in a way that is independent of the specific molecular interactions involved. For instance, in the classic experiment of a liquid filling a capillary tube, the height of the liquid in the tube is directly proportional to the curvature of the capillary tube, regardless of the interfacial energies involved.[1] Such capillary effects can be extended to explain the anisotropic shape of a liquid droplet on a grooved surface.[7,8]

The micro- and nanoscopic texture of a surface is known to influence the morphology and behavior of adherent biological cells, an effect known as contact guidance.[9] Advances in microfabrication open up promising possibilities for being able to understand and control these biological responses by means of precisely defined topographies with feature sizes that are smaller than an individual cell.[10−12] Well-studied examples include wound healing and implantology,[13−15] tissue engineering,[14,16−21] antifouling surfaces,[22] and plant−pathogen interactions.[23−32]

* To whom correspondence should be addressed. E-mail: lenhert@int.fzk.de. Present address: Forschungszentrum Karlsruhe GmbH, Institut für NanoTechnologie, 76344 Eggenstein-Leopoldshafen, Hermann-von-Helmholtz-Platz 1, Germany.

† Universitätsklinikum Münster.

‡ Physikalisches Institut, Westfälische Wilhelms-Universität.

¶ Institut für Biochemie and Biotechnologie der Pflanzen, Westfälische Wilhelms-Universität.

§ John Innes Centre.

(1) Brochard-Wyart, F. Droplets: Capillarity and wetting. In *Soft Matter Physics*; Daoud, C. E. W. M., Ed.; Springer-Verlag: Berlin, Heidelberg, New York, 1995; pp 1−45.

(2) Pierres, A.; Eymeric, P.; Baloche, E.; Touchard, D.; Benoliel, A. M.; Bongrand, P. Cell membrane alignment along adhesive surfaces: Contribution of active and passive cell processes. *Biophys. J.* **2003**, *84* (3), 2058−2070.

(3) Evans, E. Physical actions in biological adhesion. In *Structure and Dynamics of Membranes*; Lipowsky, R., Sackmann, E., Eds.; Elsevier Science: New York, 1995; Vol. 1B, pp 723−754.

(4) Sackmann, E.; Bruinsma, R. F. Cell adhesion as wetting transition? *ChemPhysChem* **2002**, *3* (3), 262−269.

(5) Legate, K. R.; Montanez, E.; Kudlacek, O.; Fassler, R. ILK, PINCH and parvin: The tIPP of integrin signalling. *Nat. Rev. Mol. Cell Biol.* **2006**, *7* (1), 20−31.

(6) Rafelski, S. M.; Theriot, J. A. Crawling toward a unified model of cell motility: Spatial and temporal regulation of actin dynamics. *Annu. Rev. Biochem.* **2004**, *73*, 209−239.

(7) Gennes, P. G. d. Wetting: Statics and dynamics. *Rev. Mod. Phys.* **1985**, *57* (3), 827−863.

(8) Cox, R. G. The spreading of a liquid on a rough solid surface. *J. Fluid Mech.* **1983**, *131*, 1−26.

(9) Curtis, A.; Wilkinson, C. Topographical control of cells. *Biomaterials* **1997**, *18*, 1573−1583.

(10) Wilkinson, C. D. W.; Curtis, A. S. G.; Crossan, J. Nanofabrication in cellular engineering. *J. Vac. Sci. Technol. B* **1998**, *16*, 3132−3136.

(11) Stevens, M. M.; George, J. H. Exploring and engineering the cell surface interface. *Science* **2005**, *310* (5751), 1135−1138.

(12) Curtis, A. S. G.; Casey, B.; Gallagher, J. O.; Pasqui, D.; Wood, M. A.; Wilkinson, C. D. W. Substratum nanotopography and the adhesion of biological cells. Are symmetry or regularity of nanotopography important? *Biophys. Chem.* **2001**, *94*, 275−283.

(13) Kotani, H.; Kawaguchi, H.; Shimoaka, T.; Iwasaka, M.; Ueno, S.; Ozawa, H.; Nakamura, K.; Hoshi, K. Strong static magnetic field stimulates bone formation to a definite orientation in vitro and in vivo. *J. Bone Miner. Res.* **2002**, *17* (10), 1814−1821.

(14) Goldner, J. S.; Bruder, J. M.; Li, G.; Gazzola, D.; Hoffman-Kim, D. Neurite bridging across micropatterned grooves. *Biomaterials* **2006**, *27* (3), 460−472.

(15) Raghavendra, S.; Wood, M. C.; Taylor, T. D. Early wound healing around endosseous implants: A review of the literature. *Int. J. Oral Maxillofacial Implants* **2005**, *20* (3), 425−431.

10.1021/la701043f CCC: $37.00 
Published on Web 08/31/2007

Although topographical contact guidance has been observed in all types of cells tested to date,[33] there are still few applications that make use of lithographically patterned surfaces. This is due to the cost of lithographic prototyping combined with the lack of an accurate model for contact guidance that would allow the design of surface patterns that are optimal for specific applications. An important first step in this direction was taken by a recent study that demonstrated an empirical correlation between the attachment of biological cells (zoospores and endothelial cells) and the surface wettability of topographically microstructured surfaces.[22] While that work correlated adhesion to topography, here we take further steps by correlating anisotropic wetting to cell orientation and growth on nanostructured surfaces. For this purpose, we have used state-of-the-art lithography to test the hypothesis that capillary effects provide a physical signal that cells can use to detect surface features, as discussed in the pioneering contact guidance works of Weiss.[34,35]

The interaction of mammalian cells with surfaces is known to be mediated by focal adhesions consisting of transmembrane integrin proteins, which transmit information across the membrane.[5,36] While passive adhesion forces and membrane deformations are sufficient to generate initial cell alignment to adhesive surfaces, active processes within the cytoskeleton such as actin polymerization quickly become involved[2] and are especially relevant to cell polarization and cell motility.[6,37] In several cases, microscopic cell protrusions known as filopodia have been observed to interact with micro- and nanoscopic surface topographies.[19,20,38,39] Model systems such as vesicles are valuable tools for the study of the physical forces involved in cell−surface interactions[40] and have provided experimental support for the idea that cell adhesion can be understood from the physical point of view of wetting transitions.[4] In the tensegrity model of cellular mechanics, molecular tension built up within the cytoskeletal network causes the cell to respond in a way that balances external mechanical forces acting upon the cell.[41] There is evidence that rearrangement of the cytoskeleton distorts the shape of the nucleus, which results in changes in gene expression.[33,42,43] This type of direct mechanotransduction is one way to explain how mechanical forces are able to switch cells between different genetic programs.[18,44,45] Indirect mechanotransduction is another mechanism involving molecular signal cascades, for instance, by means of G-proteins, kinases, and ion channels.[46,47]

Of particular interest for biomaterial surface engineering and host recognition of pathogens are geometry-specific contact guidance effects, where micro- or nanostructures on a surface induce specific cell responses. For instance, protein clustering in focal adhesions occurs on a length scale of 5−200 nm, and cells cultured on interfaces that have been chemically nanopatterned with integrin-binding RGD peptide respond preferentially to patterns below a critical length scale of about 60−75 nm.[48] The same colloidal lithography method used in that work has also been shown to be suitable for tuning the adhesion of agarose bead-based model systems using specific biotin−streptavidin interactions.[49] In order to better understand the molecular biology behind contact guidance (e.g., the role of ion channels,[50] annexins,[51] integrins,[5,36] septins and formins,[52] etc.), it is necessary to

(16) Brody, S.; Anilkumar, T.; Liliensiek, S.; Last, J. A.; Murphy, C. J.; Pandit, A. Characterizing nanoscale topography of the aortic heart valve basement membrane for tissue engineering heart valve scaffold design. *Tissue Eng.* **2006**, *12* (2), 413−421.

(17) Lenhert, S.; Meier, M. B.; Meyer, U.; Chi, L. F.; Wiesmann, H. P. Osteoblast alignment, elongation and migration on grooved polystyrene surfaces patterned by Langmuir−Blodgett lithography. *Biomaterials* **2005**, *26* (5), 563−570.

(18) Dalby, M. J.; Riehle, M. O.; Yarwood, S. J.; Wilkinson, C. D. W.; Curtis, A. S. G. Nucleus alignment and cell signaling in fibroblasts: Response to a micro-grooved topography. *Exp. Cell Res.* **2003**, *284* (2), 274−282.

(19) Dalby, M. J.; Gadegaard, N.; Riehle, M. O.; Wilkinson, C. D. W.; Curtis, A. S. G. Investigating filopodia sensing using arrays of defined nano-pits down to 35 nm diameter in size. *Int. J. Biochem. Cell Biol.* **2004**, *36* (10), 2005−2015.

(20) Dalby, M. J.; Riehle, M. O.; Johnstone, H.; Affrossman, S.; Curtis, A. S. G. Investigating the limits of filopodial sensing: A brief report using SEM to image the interaction between 10 nm high nano-topography and fibroblast filopodia. *Cell Biol. Int.* **2004**, *28* (3), 229−236.

(21) Ito, Y.; Surface micropatterning to regulate cell functions. *Biomaterials* **1999**, *20* (23−24), 2333−2342.

(22) Carman, M. L.; Estes, T. G.; Feinberg, A. W.; Schumacher, J. F.; Wilkerson, W.; Wilson, L. H.; Callow, M. E.; Callow, J. A.; Brennan, A. B. Engineered antifouling microtopographies - Correlating wettability with cell attachment. *Biofouling* **2006**, *22* (1), 11−21.

(23) Apoga, D.; Barnard, J.; Craighead, H. G.; Hoch, H. C. Quantification of substratum contact required for initiation of *Colletotrichum graminicola* appressoria. *Fungal Genet. Biol.* **2004**, *41* (1), 1−12.

(24) Tucker, S. L.; Talbot, N. J. Surface attachment and pre-penetration stage development by plant pathogenic fungi. *Annu. Rev. Phytopathol.* **2001.** *39*, 385−417.

(25) Collins, T. J.; Moerschbacher, B. M.; Read, N. D. Synergistic induction of wheat stem rust appressoria by chemical and topographical signals. *Physiol. Mol. Plant Pathol.* **2001**, *58* (6), 259−266.

(26) Read, N. D.; Kellock, L. J.; Knight, H.; Trewavas, A. J. Contact sensing during infection by fungal pathogens. In *Perspectives in Plant Cell Recognition*; Callow, J. A., Green, J. R., Eds.; Cambridge University Press: Cambridge, U.K., 1992; pp 137−172.

(27) Sesma, A.; Osbourn, A. E. The rice leaf blast pathogen undergoes developmental processes typical of root-infecting fungi. *Nature* **2004**, *431* (7008), 582−586.

(28) Talbot, N. J. On the trail of a cereal killer: Exploring the biology of *Magnaporthe grisea*. *Annu. Rev. Microbiol.* **2003**, *57*, 177−202.

(29) Jelitto, T. C.; Page, H. A.; Read, N. D. Role of external signals in regulating the pre-penetration phase of infection by the rice blast fungus, *Magnaporthe-grisea*. *Planta* **1994**, *194* (4), 471−477.

(30) Talbot, N. J.; Kershaw, M. J.; Wakley, G. E.; deVries, O. M. H.; Wessels, J. G. H.; Hamer, J. E. MPG1 encodes a fungal hydrophobin involved in surface interactions during infection-related development of *Magnaporthe grisea*. *Plant Cell* **1996.** *8* (6), 985−999.

(31) DeZwaan, T. M.; Carroll, A. M.; Valent, B.; Sweigard, J. A. *Magnaporthe grisea* Pth11p is a novel plasma membrane protein that mediates appressorium differentiation in response to inductive substrate cues. *Plant Cell* **1999**, *11* (10), 2013−2030.

(32) Zhou, X. L.; Stumpf, M. A.; Hoch, H. C.; Kung, C. A Mechanosensitive channel in whole cells and in membrane patches of the fungus *Uromyces*. *Science* **1991**, *253* (5026), 1415−1417.

(33) Dalby, M. J.; Topographically induced direct cell mechanotransduction. *Med. Eng. Phys.* **2005**, *27* (9), 730−742.

(34) Weiss, P. In vitro experiments on the factors determining the course of outgrowing nerve fiber. *J. Exp. Zool.* **1934**, *68*, 393−448.

(35) Weiss, P. Experiments on cell and axon orientation in vitro: The role of colloidal exudates in tissue organization. *J. Exp. Zool.* **1945**, *100*, 353−386.

(36) Geiger, B.; Bershadsky, A.; Pankov, R.; Yamada, K. M. Transmembrane extracellular matrix−cytoskeleton crosstalk. *Nat. Rev. Mol. Cell Biol.* **2001**, *2* (11), 793−805.

(37) Gow, N. A. R. Tip growth and polarity. In *The Growing Fungus*; Gow, N. A. R., Gadd, G. M., Eds.; Chapman & Hall: New York, 1995.

(38) Buttiglieri, S.; Pasqui, D.; Migliori, M.; Johnstone, H.; Affrossman, S.; Sereni, L.; Wratten, M. L.; Barbucci, R.; Tetta, C.; Camussi, G. Endothelization and adherence of leucocytes to nanostructured surfaces. *Biomaterials* **2003**, *24* (16), 2731−2738.

(39) Dalby, M. J.; Riehle, M. O.; Sutherland, D. S.; Agheli, H.; Curtis, A. S. G. Changes in fibroblast morphology in response to nano-columns produced by colloidal lithography. *Biomaterials* **2004**, *25* (23), 5415−5422.

(40) Pignataro, B.; Steinem, C.; Galla, H. J.; Fuchs, H.; Janshoff, A. Specific adhesion of vesicles monitored by scanning force microscopy and quartz crystal microbalance. *Biophys. J.* **2000**, *78* (1), 487−498.

(41) Ingber, D. E.; Tensegrity I. Cell structure and hierarchical systems biology. *J. Cell Sci.* **2003**, *116* (7), 1157−1173.

(42) Maniotis, A. J.; Chen, C. S.; Ingber, D. E. Demonstration of mechanical connections between integrins cytoskeletal filaments, and nucleoplasm that stabilize nuclear structure. *Proc. Natl. Acad. Sci. U.S.A.* **1997**, *94* (3), 849−854.

(43) Ingber, D. E.; Tensegrity II. How structural networks influence cellular information processing networks. *J. Cell Sci.* **2003**, *116* (8), 1397−1408.

(44) Engler, A. J.; Sen, S.; Sweeney, H. L.; Discher, D. E. Matrix elasticity directs stem cell lineage specification. *Cell* **2006**, *126* (4), 677−689.

(45) Feng, L.; Li, S. H.; Li, Y. S.; Li, H. J.; Zhang, L. J.; Zhai, J.; Song, Y. L.; Liu, B. Q.; Jiang, L.; Zhu, D. B. Super-hydrophobic surfaces: From natural to artificial. *Adv. Mater.* **2002**, *14* (24), 1857−1860.

(46) Li, C. H.; Xu, Q. B. Mechanical stress-initiated signal transductions in vascular smooth muscle cells. *Cell. Signalling* **2000**, *12* (7), 435−445.

(47) Rajnicek, A. M.; McCaig, C. D. Guidance of CNS growth cones by substratum grooves and ridges: Effects of inhibitors of the cytoskeleton, calcium channels and signal transduction pathways. *J. Cell Sci.* **1997**, *110*, 2915−2924.

(48) Arnold, M.; Cavalcanti-Adam, E. A.; Glass, R.; Blummel, J.; Eck, W.; Kantlehner, M.; Kessler, H.; Spatz, J. P. Activation of integrin function by nanopatterned adhesive interfaces. *ChemPhysChem* **2004**, *5* (3), 383−388.

(49) Selhuber, C.; Blummel, J.; Czerwinski, F.; Spatz, J. P. Tuning surface energies with nanopatterned substrates. *Nano Lett.* **2006**, *6* (2), 267−270.

distinguish between purely physical contact guidance effects and those that appear to require specific molecular machinery in order to function.

A requirement for direct comparison between the behavior of macroscopic liquid droplets and microscopic cells is a topographical pattern with features that are significantly smaller than a single cell. The pattern must also be continuous over length scales that are large enough for sessile drop measurements. Langmuir−Blodgett (LB) lithography is particularly suitable for both anisotropic wettability measurements[53] and cell alignment assays[17] because it allows the rapid and cheap fabrication of a range of chemically identical substrates, each having surface areas of several square centimeters with groove dimensions that are significantly smaller than an individual cell.[54] The depth of the grooves can be controlled between 20 and 300 nm by the etch time, while the lateral line widths can be tuned from 100 nm to more than 2 $\mu$m.[55]

Osteoblasts line the surface of bone in vivo. They are responsible for bone formation and are therefore the focus of many clinical treatments of bone breaks and tissue engineering. Although little is known about the relationship between osteoblast alignment and function in vivo, there is evidence that their alignment on bone surfaces as well as synthetic implants is important for the generation of bone tissue. For instance, osteoblasts have been observed to align in vitro under strong magnetic fields, and the same fields were found to induce directed bone growth in vivo.[13] Osteoblasts cultured on regularly spaced grooves of subcellular dimensions show a tendency to form focal adhesions at opposite ends of aligned cells and to migrate more quickly in the direction of alignment.[17] Although deeper grooves have been observed to yield stronger osteoblast alignment, a systematic study of the dependence on groove depth, width, and pitch is necessary for a more complete understanding of the relevant physical parameters involved in contact guidance.

Detection of the physicochemical features of surfaces is also important for infection of plants by fungal pathogens, which differ from animal cells in having a cell wall. A well-documented example of topographical contact guidance of a fungal pathogen occurs when spores of the stem rust fungus *Puccinia graminis* germinate on cereal leaves. In this case, the germ tubes grow perpendicular to the veins of the leaf in order to optimize the chances of encountering a stoma, through which the fungus is able to invade the plant after forming infection structures (appressoria).[26,56] This developmental process can be simulated on artificial surfaces with microscopically grooved topographies that mimic the geometric dimensions of guard cells on the leaf surface.[25,57] However, quantitative studies of *P. graminis* alignment as a function of groove dimensions or on smooth chemically patterned surfaces are lacking. Knowledge of the biological mechanisms required for surface recognition and alignment will enable us to establish which surface cues are involved and whether germ tube alignment is a feasible target for plant protection strategies.

The rice blast fungus *Magnaporthe grisea* also senses the surface of its host in order to form penetration structures: elaborate, heavily melanized appressoria on leaf surfaces[28] and structures resembling simple appressoria (hyphopodia) on roots.[27] The amenability of *M. grisea* to genetic transformation has provided some insight into the molecular mechanisms by which this organism is able to detect surface cues.[28] For example, PTH11 is a transmembrane protein identified through an insertional mutagenesis screen for nonpathogenic mutants. PTH11 mutants are strongly reduced in appressorium formation, and the gene product has been suggested to be involved in host surface recognition.[31] MPG1 encodes for a hydrophobin, a small hydrophobic cell surface protein that is highly expressed during the first steps of host plant infection. Mutants defective in this hydrophobin have reduced virulence and are defective in conidiation and appressorium formation.[58] *M. grisea* differs from *P. graminis* in that it is able to penetrate directly through the plant epidermis, apparently without a requirement for extensive surface navigation. Although appressoria formation in *M. grisea* has been studied in considerable detail,[24,29] to our knowledge, the alignment behavior of *M. grisea* germ tubes on surfaces has not yet been documented.

Although the mechanisms by which cells detect and transduce topographical information are not yet well understood,[33] the effect that surface topography will have on the shape of a pure liquid droplet is predictable from established physical descriptions.[1] In order to distinguish cell-specific effects from behavior that may be induced by capillary forces, we have compared the spreading of water droplets with the alignment of three different types of biological cells. Osteoblasts are an example of an animal cell that has been observed to align on grooves of subcellular lateral dimensions. *P. graminis* and *M. grisea* germ tubes are examples of fungal hyphae, both of which are known to detect surface cues.

## Materials and Methods

**Surface Fabrication.** A combination of LB lithography and nanoimprinting was used to continuously pattern polystyrene surface areas of more than 4 cm$^2$ with regularly spaced grooves, as described.[54] In order to fabricate striped patterns with different lateral dimensions,[55] the transfer speed was varied between 1 and 60 mm/min, and the surface pressure was varied between 0 and 5 mN/m. The groove depth was controlled by the etch time. The chemically striped (octadecyltrichlorosilane (OTS)) patterns were prepared by excluding the etching step. The grooved silicon templates were then used for production of the polystyrene replicas by hot embossing as described.[54] The lateral size and thickness of the sample can be controlled by the amount of polystyrene used and the time used for embossing. In this case, samples were approximately 4 cm$^2$ and 1 mm thick. Polystyrene surfaces were made hydrophilic for the anisotropic wettability studies as well as the osteoblast and *M. grisea* cell culture using a 50 W $O_2$ plasma (Templa System 100-E plasma system) at 1 mbar for 10 s. For the osteoblast culture, the surfaces were sterilized by immersion in 70% ethanol for 5 min.

**Topographical Measurements.** SFM investigations were performed with a commercial instrument (Nanoscope IIIa and Dimension 3000, Digital Instruments, Santa Barbara, CA) operating in tapping

(50) Hamill, O. P.; Martinac, B. Molecular basis of mechanotransduction in living cells. *Physiol. Rev.* **2001**, *81* (2), 685−740.

(51) Gerke, V.; Creutz, C. E.; Moss, S. E. Annexins: Linking Ca2+ signalling to membrane dynamics. *Nat. Rev. Mol. Cell Biol.* **2005**, *6* (6), 449−461.

(52) Gladfelter, A. S. Control of filamentous fungal cell shape by septins and formins. *Nat. Rev. Microbiol.* **2006**, *4* (3), 223−229.

(53) Gleiche, M.; Chi, L. F.; Gedig, E.; Fuchs, H. Anisotropic contact-angle hysteresis of chemically nanostructured surfaces. *ChemPhysChem* **2001**, *2* (3), 187−191.

(54) Lenhert, S.; Zhang, L.; Mueller, J.; Wiesmann, H. P.; Erker, G.; Fuchs, H.; Chi, L. F. Self-organized complex patterning: Langmuir−Blodgett lithography. *Adv. Mater.* **2004**, *16* (7), 619−624.

(55) Lenhert, S.; Gleiche, M.; Fuchs, H.; Chi, L. F. Mechanism of regular pattern formation in reactive dewetting. *ChemPhysChem* **2005**, *6* (12), 2495−2498.

(56) Read, N. D.; Kellock, L. J.; Collins, T. J.; Gundlach, A. M. Role of topography sensing for infection-structure differentiation in cereal rust fungi. *Planta* **1997**, *202* (2), 163−170.

(57) Allen, E. A.; Hazen, B. E.; Hoch, H. C.; Kwon, Y.; Leinhos, G. M. E.; Staples, R. C.; Stumpf, M. A.; Terhume, B. T. Appressorium formation in response to topographical signals by 27 rust species. *Phytopathology* **1991**, *81* (3), 323−331.

(58) Talbot, N. J.; Ebbole, D. J.; Hamer, J. E. Identification and characterization of Mpg1, a gene involved in pathogenicity from the rice blast fungus *Magnaporthe-grisea*. *Plant Cell* **1993**, *5* (11), 1575−1590.

mode (silicon cantilevers, Nanosensors) with resonant frequencies of 250−350 kHz and nominal spring constants of ∼42 N/m. Since the grooves have a sidewall angle of 54.7°, the groove width and ridge width was measured at 1/2 of the groove depth. From these dimensions, the roughness factor can be calculated with the following formula:

$$[2 - 2\cos(54.7°)](\text{pitch} + \text{depth})/[\text{pitch}\cdot\sin(54.7°)] \quad (1)$$

**Anisotropic Wetting Measurements.** Water drop anisotropy was measured by placing 13 0.5 $\mu$L drops of hemalaun dye (Sigma-Aldrich) solution in water from an Eppendorf pipet onto each substrate and leaving the drops to spread in ambient conditions until dry. Photographs were then taken of the resulting drop residue, and the aspect ratio (anisotropy) was calculated for each drop by dividing the length of the drop in the groove direction by the width of the drop perpendicular to the grooves. Dynamic contact angles were measured using a commercial instrument (G2 Kontaktwinkelmess-system, Krüss). Advancing contact angles were determined by fitting a polynomial to the shape of the drop photographed from the side as it increased and decreased in size between volumes of 30−100 $\mu$L, at intervals of 1 $\mu$L/image. In the case of the chemical stripes, the water drop anisotropy was calculated from the dynamic contact angles measured as the contact line moved parallel and perpendicular to the stripes. For this purpose, formulas 2 and 3 were derived from geometric principles in order to relate the contact angles to the aspect ratio of the drops. If we assume circular cross sections of the drop, then the length ($L$) to width ($W$) ratio of the drop can be expressed in terms of the contact angles for pairs of angles greater than 90° by

$$\frac{L}{W} = \frac{\dfrac{1 + \cos(180 - \Theta_w)}{1 + \cos(180 - \Theta_l)}[\sin(180 - \Theta_l)]}{\sin(180 - \Theta_w)} \quad (2)$$

or, in the case where the contact angles are less than 90°, by

$$\frac{L}{W} = \frac{\dfrac{1 + \sin(90 - \Theta_w)}{1 + \sin(90 - \Theta_l)}[\cos(90 - \Theta_l)]}{\cos(90 - \Theta_w)} \quad (3)$$

$\Theta_l$ and $\Theta_w$ represent the contact angles corresponding to the long and short axis of the drop, respectively. All wetting measurements were repeated three to five times.

**Osteoblast Culture and Analysis.** Osteoblasts were cultured for 24 h in high growth enhancement medium (ICN Biomedicals GmbH, Eschwege, Germany) supplemented with 10% fetal calf serum, 250 mg/mL amphotericin B, 10 000 IU/mL penicillin, 10 000 mg/mL streptomycin, and 200 mM L-glutamine (Biochrom KG seromed, Berlin, Germany) using a cell density of 2000 cells/cm$^2$. The cultures were incubated at 37 °C in a humidified atmosphere of 95% air and 5% $CO_2$. The cells were fixed with glutaraldehyde and stained with toluidine blue in order to provide contrast for optical microscopy and analysis of cell orientation, as described.[17] Micrographs were taken from at least eight different areas per sample for image analysis. The osteoblast anisotropy was defined as the length of the cell (in the direction of the grooves) divided by the width (perpendicular to the grooves). At least 100 cells were counted per measurement, and the experiment was performed in triplicate.

**Culture and Analysis of Fungi.** Uredospores of *P. graminis* f. sp. *tritici* race 32 were prepared as described,[59] and the artificial surfaces were inoculated using a settling tower. *M. grisea* wild type and mutant strains Guy11, 4091.5.8, *mpg1*, and *pth11* were cultured and maintained as described.[58] Drops of water (300−400 $\mu$L) containing $10^3$ conidia/mL were placed on the surfaces. The fungal spores were incubated for 8−12 (*M. grisea*) or 24 (*P. graminis*) hours at 23 °C and 100% relative humidity. For fluorescence microscopy, germ tubes were stained with calcofluor and either imaged under liquid or after drying under a stream of compressed nitrogen gas. No observable change in the orientation of the germ tubes could be detected in cells that were viewed under a microscope both before and after this drying process. Micrographs for image analysis were taken of at least 100 cells per surface in the case of *P. graminis* and at least 200 cells per surface in the case of *M. grisea*. The experiments were repeated three and four times.

**Image Analysis.** Cell orientation of the osteoblasts and *P. graminis* was quantified using ImageJ (version 1.61, by Wayne Rasband; NIH, Bethesda, MD). An ellipse was fitted to the shape of each cell, and the orientation of the major axis of the ellipse was assumed to be the orientation of the cells. In order to speed up the image analysis process for the experiments with *M. grisea* (wild types and mutants), customized image analysis software was developed. Briefly, this software recognizes each cell in an optical micrograph by means of a threshold function, and fits a straight line through it based on a linear regression over all points that form the shape. After that, the angle of this straight line in respect to the groove orientation is calculated. For all cell types, only the cells that were not in direct contact with neighboring cells were counted. We define "alignment" as the percentage of cells that are oriented within 30° of the groove direction. A randomly oriented distribution as is expected in the controls (surface #1) should show 33% alignment.

**Statistics.** Linear regressions and ANOVA tables were calculated using Origin 6.1. $p$-Values represent the probability that the correlation coefficient ($r$) is zero. In the cases where data points were excluded from the linear regression, the $p$-values represent conditional probabilities, with the condition being that either the roughness factor or individual groove volume is below a critical value. The Student's $t$ test was used to test for significant alignment on the chemical patterns. All error bars and ± values represent the standard deviation.

## Results

**Surface Characterization.** The width, depth, and pitch of the grooved topographies were measured by scanning force microscopy (Figure 1 and Table 1). From these measurements, roughness factors and individual groove volumes were calculated. These two parameters were found to be most relevant to the cell and water-drop experiments described herein. The roughness factor as defined by Wenzel is a unitless number that gives the real surface area when multiplied by the apparent surface area.[60] In the case of the microscopic grooves used here, this roughness factor is determined by the groove dimensions and is therefore anisotropic.

The anisotropic wettability of the surfaces was measured using a classical method in which sessile drops of water are placed on the surface and allowed to spread (Figure 2a).[1] We define the "water drop anisotropy" as the drop length in the groove direction divided by the length perpendicular to the grooves, which can be measured from photographs of the droplets (Figure 2a). Linear regression analysis of the water drop anisotropy as a function of the geometric parameters shown in Table 1 results in the following correlation coefficients ($r$) and $p$-values: depth ($r = 0.64$, $p = 0.025$), groove width ($r = -0.75$, $p = 7.3 \times 10^{-3}$), ridge width ($r = -0.71$, $p = 0.017$), pitch ($r = -0.77$ $p = 5.3 \times 10^{-3}$), roughness factor ($r = 0.93$, $p < 10^{-4}$), groove volume ($r = -0.23$, $p = 0.48$). The best correlation is clearly observed with the roughness factor. Plotting water drop anisotropy against the roughness factor (Figure 2b) for roughness factor values below 1.2 reveals a strictly linear correlation ($r = 0.99$). Beyond this roughness value, the trend begins to deviate slightly from linearity but still provides a reasonable means of predicting the anisotropic wettability from the groove dimensions (with $p <$

(59) Moerschbacher, B. M.; Noll, U.; Gorrichon, L.; Reisener, H. J. Specific-inhibition of lignification breaks hypersensitive resistance of wheat to stem rust. *Plant Physiol.* **1990**, *93* (2), 465−470.

(60) Wenzel, R. N. Resistance of solid surfaces to wetting by water. *Ind. Eng. Chem.* **1936**, 28, 988−994.

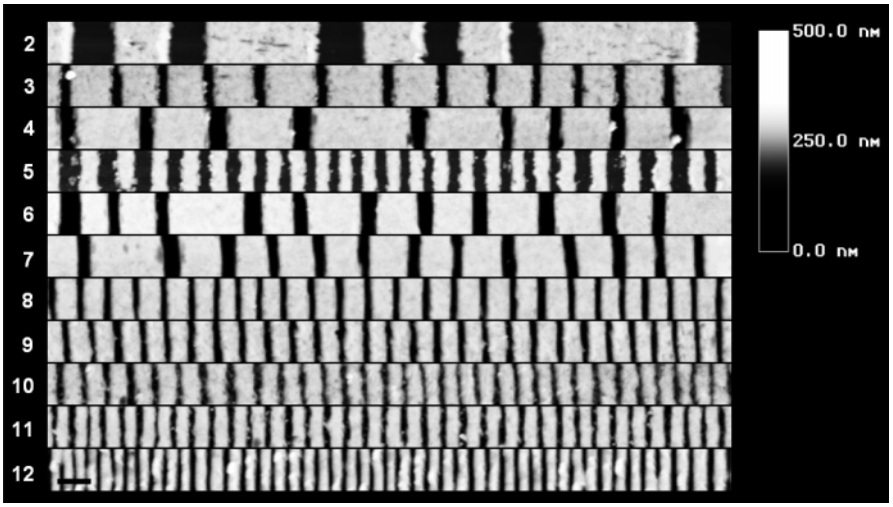


**Figure 1.** Topographical scanning force micrographs of the different grooved polystyrene topographies. The topographies are numbered from 2 to 12, and correspond to the sample numbers in Table 1. Scale bar = 1 $\mu$m.

**Table 1. Topographical Dimensions of the Grooved Surfaces, as Determined by Scanning Force Microscopy (Representative Measurements Are Shown in Figure 1)[a]**

| surface # | roughness factor | groove depth (nm) | groove width (nm) | ridge width (nm) | pitch (nm) | groove volume (fl/$\mu$m) |
|---|---|---|---|---|---|---|
| 1 | 1 | 0 | | | | 0 |
| 2 | 1.04 ± 0.11 | 105 ± 8 | 1200 ± 150 | 1650 ± 170 | 2850 ± 220 | 126.0 ±18 |
| 3 | 1.08 ± 0.16 | 119 ± 15 | 316 ± 76 | 1180 ± 140 | 1500 ± 160 | 37.6 ± 10 |
| 4 | 1.12 ± 0.34 | 194 ± 13 | 410 ± 73 | 1280 ± 380 | 1690 ± 390 | 79.5 ± 15 |
| 5 | 1.14 ± 0.25 | 116 ± 27 | 424 ± 130 | 424 ± 62 | 848 ± 140 | 49.2 ± 19 |
| 6 | 1.18 ± 0.36 | 241 ± 40 | 289 ± 69 | 1140 ± 320 | 1420 ± 330 | 69.6 ± 20 |
| 7 | 1.20 ± 0.15 | 258 ± 18 | 235 ± 18 | 1080 ± 120 | 1310 ± 120 | 60.6 ± 6.3 |
| 8 | 1.20 ± 0.12 | 138 ± 12 | 152 ± 18 | 548 ± 48 | 700 ± 51 | 21.0 ± 3.1 |
| 9 | 1.21 ± 0.21 | 132 ± 16 | 121 ± 22 | 520 ± 84 | 641 ± 87 | 16.0 ± 3.5 |
| 10 | 1.22 ± 0.25 | 118 ± 17 | 156 ± 37 | 402 ± 79 | 558 ± 87 | 18.4 ± 5.1 |
| 11 | 1.26 ± 0.13 | 141 ± 7 | 150 ± 19 | 417 ± 40 | 567 ± 44 | 21.2 ± 2.9 |
| 12 | 1.37 ± 0.15 | 155 ± 23 | 122 ± 14 | 316 ± 34 | 438 ± 37 | 18.9 ± 3.6 |

[a] The values are sorted according to the roughness factor, which was calculated from the measured groove dimensions. The ± values represent the standard deviation between measurements from eight random areas of the substrate.

$10^{-4}$). Both hydrophilic (Figure 2b) and hydrophobic (Supporting Information Figure S1) surfaces show the same trends.

**Mammalian Osteoblasts**. Like water drops, osteoblasts align parallel to the groove direction to different extents on different surfaces. Figure 3a shows an extreme example of an aligned osteoblast on surface #12. A significant correlation was observed between the osteoblast anisotropy and the water drop anisotropy ($r = 0.77$ $p = 3.3 \times 10^{-3}$; Figure 4). It can be seen that three data points (circled in Figure 4) were slightly below the trendline. Although a $p$-value of less than 0.01 is observed when all data points are included, exclusion of surfaces with roughness factors greater than 1.22 (#10−12) from the linear regression results in a 5-fold increase in the significance of the correlation ($r = 0.91$, $p = 6.8 \times 10^{-4}$). This $p$-value represents the roughness-conditional probability of a correlation below a critical roughness factor of 1.22, indicating that the three roughest surfaces induce slightly less alignment than predicted by the water drop anisotropy.

***P. graminis* Germ Tubes.** In contrast to osteoblast cells, which align parallel to the groove direction, the overall growth direction of germ tubes of *P. graminis* is perpendicular to the grooves (Figure 3b). Although a variety of interesting germ tube morphologies were observed, including branching, zig-zagging, and straight growth (all observable in the same germ tube in Figure 3b and also seen in germ tubes growing on flat control surfaces), we focused our statistical analysis only on the orientation of the entire germ tube as described in the methods for the sake of automated image analysis. No significant correlation was observed when *P. graminis* germ tube alignment was compared with water drop anisotropy when considering all data points ($r = 0.16$, $p = 0.62$, solid line in Figure 5a). However, four topographies (#2, 4, 6, 7) showed a stronger alignment than expected from the water drop anisotropy alone. These four topographies were the ones with the largest groove volumes (Table 1). When the data were reanalyzed for groove volumes of less than 60 fL/$\mu$m (Figure 5; Table 1) there was a significant correlation between germ tube alignment and water drop anisotropy ($p < 0.05$).

As a complementary test of the idea that capillary effects can affect the cell alignment of *P. graminis* (even in the absence of topography), we fabricated chemically striped surfaces consisting of parallel lines of hydrophobic OTS separated by gaps of hydrophilic silicon oxide. Since these chemical patterns exert anisotropic capillary forces on pure liquid droplets,[53] yet have a "groove volume" of zero, they can be used to test the hypothesis that grooves with volumes of less than 60 fL/$\mu$m induce germ tube alignment by capillary forces alone. In this case, the water drop anisotropy was calculated from advancing contact angle measurements using pure water so that the data could be shown as the triangles in Figure 5a. Only two data points are included here because only a slight water drop anisotropy (of ~1.05) can be measured on these surfaces. Nevertheless, we found a small but significant difference in germ tube alignment between the OTS-covered control and the chemically striped surfaces (illustrated in Figure 5; "otsc" = control; "ots" = chemically

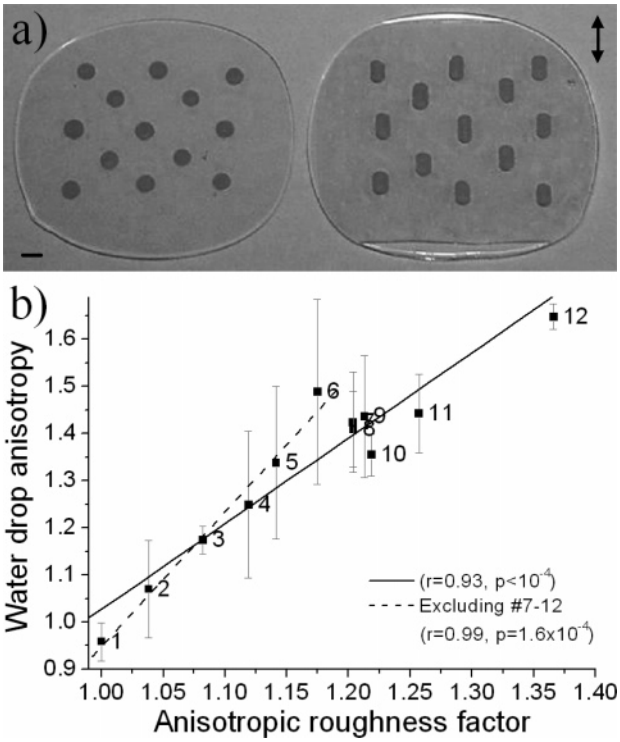


**Figure 2.** Water drop anisotropy. (a) Photographs of the anisotropic spreading of dye-containing water droplets on a smooth control surface (left, surface #1) and a grooved surface (right, surface #12). The double headed arrow shows the orientation of the grooves. Scale bar = 1 mm. (b) The water drop anisotropy is plotted as a function of the roughness factor for surfaces #1−12 (Table 1). The solid line shows the linear regression of the whole data set, and the dotted line shows the linear regression excluding data points #7−12. Correlation coefficients ($r$) and $p$-values are shown for both.

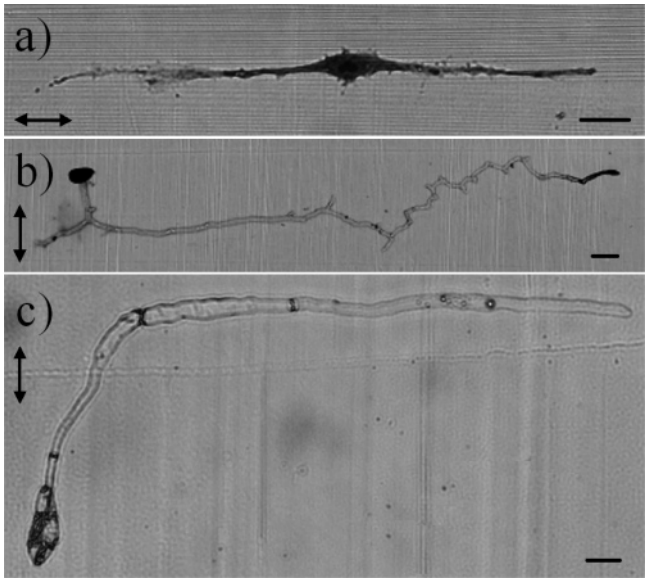


**Figure 3.** Optical micrographs of aligned osteoblast cells and fungal germ tubes. (a) An osteoblast aligned parallel to the grooves. (b) *P. graminis* and (c) *M. grisea* germ tubes aligned perpendicular to the grooves. The surface in all three cases is #12. The orientation of the grooves is indicated by double-headed arrows. Scale bars = 10 $\mu$m.

striped surface) ($p < 0.05$). These findings indicate that chemically striped surfaces can induce germ tube alignment even though they have a groove volume of zero.

***M. grisea* Germ Tubes.** Unlike *P. graminis*, there is no obvious survival-based reason for *M. grisea* hyphae to align with host

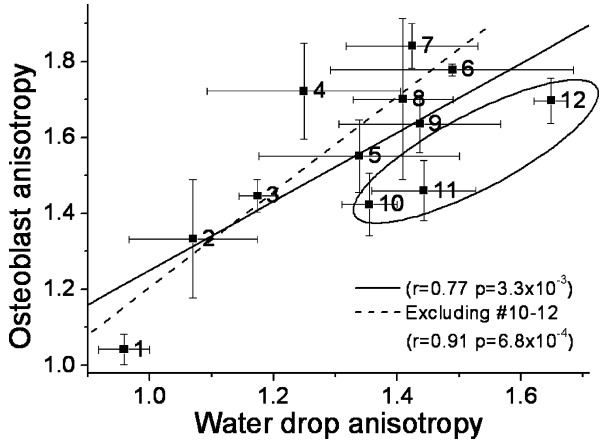


**Figure 4.** Correlation between the osteoblast anisotropy and the water drop anisotropy on different surface topographies. The solid line shows the linear regression of the data set, and the dotted line shows the conditional correlation excluding the highlighted data points (surfaces #10−12). Correlation coefficients ($r$) and $p$-values are shown for both.

surface features. Surprisingly, germ tubes of *M. grisea* also showed a statistically significant tendency for an overall growth direction perpendicular to the various grooved topographies in Table 1. An example of an aligned *M. grisea* germ tube cultured on hydrophilic grooves is shown in Figure 3c. A significant correlation was observed between *M. grisea* germ tube alignment and water drop anisotropy across all data points ($r = 0.84$, $p = 7.1 \times 10^{-4}$; Figure 6). This alignment was not dependent on genes that have previously been shown to be required for surface-sensing mechanisms that lead to appressorial differentiation since germ tubes of the hydrophobin mutant *mpg1*[30] and the plasma membrane protein mutant *pth11*[31] showed perpendicular germ tube alignment on hydrophilic and hydrophobic surfaces, as did the corresponding wild-type strains (Guy11 and 4091-5-8, respectively). In the case of *M. grisea*, hydrophobic surfaces simulate leaf infection,[28,45] while hydrophilic surfaces simulate root infection.[27] While classical appressoria typical for leaf penetration formed on hydrophobic substrates (not shown), thickened germ tubes typical for root penetration were observed on the hydrophilic substrates (Figure 3c). However, no qualitative differences in morphology (besides alignment) were observed as a result of the absence or presence of grooves or of groove dimensions on both types of substrates. Cryo-scanning electron microscopy (cryo-SEM) imaging indicated that the germ-tubes grew in close contact with the substrates (Supporting Information Figure S3). In all cases, perpendicular alignment was correlated with water drop anisotropy ($p < 0.05$) (Supporting Information Figure S2). Only in the case of the 4091-5-8 wild type on hydrophobic grooves was a conditional correlation observed, where exclusion of the roughest sample #12 resulted in $p < 0.05$. This suggests that capillary forces are the dominant physical parameter that governs the alignment of *M. grisea* germ tubes.

## Discussion

The anisotropic spreading of liquid drops on anisotropic surfaces has, to our knowledge, not been considered in studies that investigate the effects of substrate surface energy or topography in cell adhesion. Even in pure physical studies, the experimental situation has, so far, only confirmed the theory in the case of spreading in one direction, i.e., parallel to the grooves.[61]

(61) Gerdes, S.; Cazabat, A. M.; Strom, G. The spreading of silicone oil droplets on a surface with parallel V-shaped grooves. *Langmuir* **1997**, *13* (26), 7258−7264.

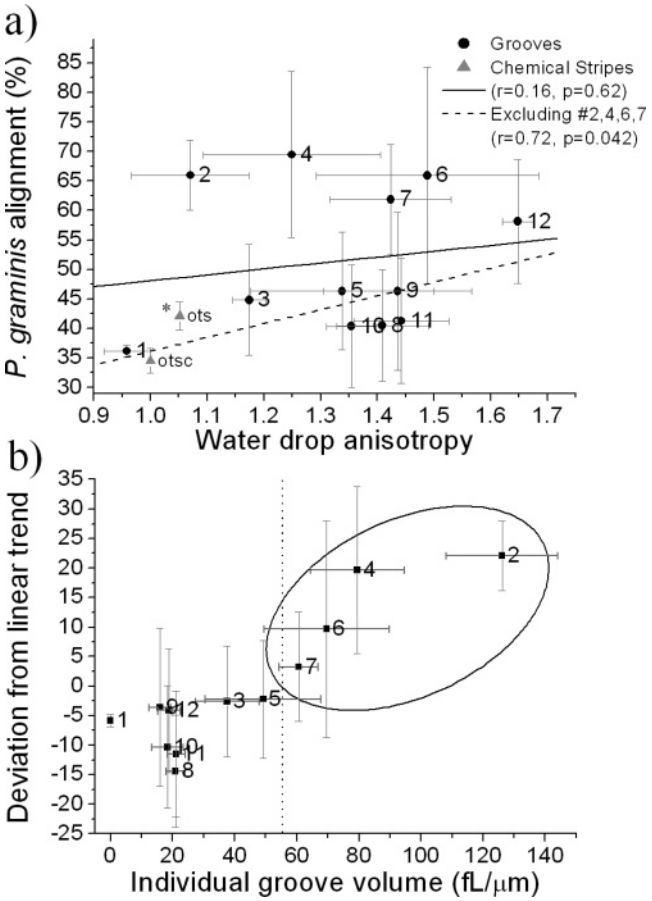


**Figure 5.** *P. graminis* alignment. (a) Correlation between the cell alignment and the water drop anisotropy on the different surface topographies. The solid line shows the linear regression of the data set, and the dotted line shows the conditional correlation excluding data points #2, 4, 6, and 7. Correlation coefficients ($r$) and $p$-values are shown for both. Triangles show the alignment and water drop anisotropies on chemically heterogeneous, striped surfaces (ots) compared with five chemically homogeneous controls (otsc). A significant difference ($p < 0.05$, Student's $t$ test) from the control is indicated with an asterisk (*). (b) Deviation from the dotted trend line in panel a is shown as a function of groove volume. The largest deviation is observed for grooves with volumes larger than 55 fL/$\mu$m.

Here we have shown that there is a linear relationship between droplet anisotropy and the anisotropic surface roughness (Figure 2). This finding makes it possible to approximate the relative anisotropic wettability from the known groove dimensions, so allowing one to test the hypothesis that capillary forces influence cell alignment without the immediate need for direct anisotropic wetting measurements. The linear dependence of the water drop anisotropy (or the ratio between spreading parallel and perpendicular to the grooves) on the anisotropic roughness factor is predicted for the theoretical description of droplet spreading on sinusoidal grooves.[8] As this theory is only valid for low roughness factors, we do not yet have a theoretical explanation for the slight deviation from strict linearity observed at higher roughness factors. As the theory predicts,[8] the same qualitative trends were observed for both hydrophilic and hydrophobic surfaces, making it possible to use a single liquid/substrate combination for direct comparison with the cell alignment. The idea that capillary forces can influence cell shape in a way independent of specific molecular interactions is not only applicable to cells cultured on topographically grooved surfaces, but also on fibers, in capillary tubes, and possibly on chemical patterns as well.[1,8,9,21,62]

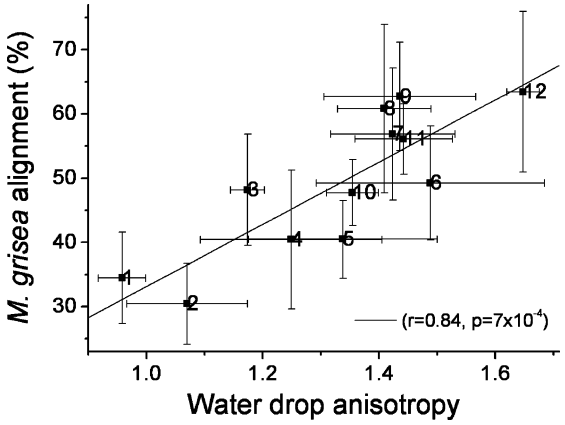


**Figure 6.** Correlation between the alignment of M. *grisea* germ tubes (Guy11 strain) and water drop anisotropy on different surface topographies. The regression line, correlation coefficients ($r$), and $p$-values are shown.

The alignment of osteoblasts on the topographically grooved patterns used here appeared to be primarily governed by capillary forces. The observation that the grooved surfaces with the largest roughness factors induced slightly less osteoblast alignment than predicted by the water drop anisotropy measurements is consistent with the idea that the plasma membrane follows the surface topography, but cannot bend sufficiently to follow very rough surfaces. This phenomenon has been directly measured by interference reflection microscopy in the case of fibroblasts.[63] A strikingly similar effect can be observed when one compares the water drop anisotropy on hydrophilic grooves with that of hydrophobic grooves (Supporting Information Figure S1), which can be described in physical terms by the Cassie effect that leads to superhydrophobicity.[45,64] The observation that capillary forces are sufficient to align mammalian cells such as osteoblasts suggests that increased understanding and ability to control these fundamental physical forces in vivo can be directly translated into improvements in clinical treatments.[16]

The phytopathogenic fungus *P. graminis* differs from the other cell types used here in that its fitness as a plant pathogen is known to be related to its ability to detect topographical features of a substrate, such as grooves present on the surface of a wheat leaf. A previous study showed that over 90% of the germ tubes differentiate appressoria upon encountering a stoma in vivo, and microfabricated grooves of dimensions comparable to the guard cells of cereal stomatal complexes (2 $\mu$m depth with spacings of 1.5 $\mu$m) have been found to induce about 85% differentiation, indicating that *P. graminis* is able to detect and respond to specific topographical geometries.[56] This is consistent with our observation that certain topographies gave a significantly enhanced response, suggesting that these topographies act upon a particular signaling pathway. It is known that a similar topography sensing fungus (*Uromyces appendiculatus*) contains mechanosensitive $Ca^{2+}$ ion channels in the cell membrane that are sensitive to mechanical deformation of the membrane such as bending or area expansion.[32,50] It is therefore conceivable that the extracellular matrix and cell wall of the fungus could fill up the smaller grooves until a critical volume, after which membrane bending over the edges and the corresponding signal transduction can be expected to

(62) Gleiche, M.; Chi, L. F.; Fuchs, H. Nanoscopic channel lattices with controlled anisotropic wetting. *Nature* **2000**, *403* (6766), 173−175.
(63) Walboomers, X. F.; Monaghan, W.; Curtis, A. S. G.; Jansen, J. A. Attachment of fibroblasts on smooth and microgrooved polystyrene. *J. Biomed. Mater. Res.* **1999**, *46* (2), 212−220.
(64) McHale, G.; Shirtcliffe, N. J.; Aqil, S.; Perry, C. C. Newton, M. I. Topography driven spreading. *Phys. Rev. Lett.* **2004**, *93* (3), 036102.

occur. However, based on this alignment mechanism alone, it is difficult to explain how the smaller grooves have any effect on the hyphal alignment at all, since the cell wall and adhesion pad of the fungus separate the membrane from the substrate by several hundred nanometers. This, together with the observation that smooth chemical patterns can also induce a slight alignment of *P. graminis*, suggests that the anisotropic wettability has a basic effect on the cell, independent of the topographically induced bending of the membrane. Importantly, it would have been impossible to determine the critical groove volume that induces this effect (60 fL/$\mu$m) without considering the capillary-induced contact guidance as a background.

The data for *M. grisea* germ tubes provide further evidence that topographically induced capillary forces are sufficient for alignment of fungal germ tubes. Since *M. grisea* has the ability to penetrate plant surfaces directly through the leaf cuticle or root epidermis, there is no obvious need for this fungus to carry out extensive surface navigation prior to penetration. Furthermore, mutants that are defective in pathogenesis-related differentiation on plant surfaces showed perpendicular germ tube alignment on grooved surfaces, the degree of alignment being predictable as a function of anisotropic wettability. Collectively, these data suggest that *M. grisea* alignment is governed by capillary effects and is independent of host-specific surface sensing events. This is consistent with previous *in planta* experiments that showed no differences in appressorium formation by *M. grisea* on host or non-host plants.[65]

The observation that cells are able to detect and respond to capillary forces raises the question of what role these forces may play in vivo. Cells are known to detect complex chemical and physical information from extracellular interfaces and matrices, and are able to use this information to determine behavior ranging from growth direction to differentiation.[36,44] Well-studied examples of anisotropy in extracellular materials include the micro- and nanoscopic topographies of plant leaves resulting in anisotropic superhydrophobicity[45] and self-assembling collagen fibrils exhibiting anisotropy on a variety of scales depending on the type of tissue.[66] Capillary-induced contact guidance may provide a physical basis for cells to detect and respond, not only to the presence of particular molecules and interfaces, but also to their supramolecular organization, which can be simplified in vitro by topographical and chemical patterning. A promising approach to the understanding of capillary-induced contact guidance in vivo is therefore to quantify the physical−chemical properties of biological materials that may be expected to lead to capillary forces on length scales well below the 10 $\mu$m scale of individual cells (for example, anisotropy, roughness, curvature, elasticity, and chemical contrast, to name a few).

## Conclusions

We have proposed a general physical mechanism for contact guidance based on the fundamental physical phenomenon of droplet spreading and tested it with three well-studied cell types. In all cases, capillary forces are found to be sufficient to induce cell alignment. Our hypothesis is relatively simple to test in the case of grooves that are significantly smaller than an individual cell, as calculation of the anisotropic roughness factor is a good predictor of the anisotropic wettability. Deviations from this model provide insight into cell-specific geometry effects and mechanotransduction by mechanisms such as membrane bending or expansion, providing a useful method for studies that seek to unravel the mechanisms by which biological cells interact with a surface.

**Acknowledgment.** We thank N. Talbot and B. Valent for *mpg1* and *pth11* strains, U. Beike for providing *P. graminis* spores, I. Gabriniok and M.-B. Meier for help with the osteoblast cell culture, and M. Dirks and N. van Deenen for help with the analysis of the *M. grisea* data. S.L. thanks the DFG (WI1769) for financial support.

**Supporting Information Available:** Water drop anisotropy on hydrophobic grooves, complete data for mutant and wild-type *M. grisea* alignment, and cryo-SEM image of an *M. grisea* germ tube. This material is available free of charge via the Internet at http://pubs.acs.org.

LA701043F

(65) Gilbert, R. D.; Johnson, A. M.; Dean, R. A. Chemical signals responsible for appressorium formation in the rice blast fungus *Magnaporthe grisea*. *Physiol. Mol. Plant Pathol.* **1996**, *48* (5), 335−346.

(66) Ottani, V.; Raspanti, M.; Ruggeri, A. Collagen structure and functional implications. *Micron* **2001**, *32* (3), 251−260.